Journal of the Ceramic Society of Japan 121 [12] 992-998 2013 Paper

Hydrothermal stability of hydrogen permselective amorphous silica membrane synthesized by counter diffusion chemical vapor deposition method

Keita MIYAJIMA,[*,,†] Tomokazu EDA,[**] Balagopal N. NAIR,[**] Sawao HONDA[*] and Yuji IWAMOTO[*]**

[*]**Department of Frontier Materials, Graduate School of Engineering, Nagoya Institute of Technology, Gokiso-cho, Showa-ku, Nagoya 466–8555, Japan**

[**]**Research and Development Center, Noritake Co., Limited, 300 Higashiyama, Miyoshi-cho, Miyoshi, Aichi 470–0293, Japan**

Hydrogen-permselective amorphous silica membranes were synthesized by the counter diffusion chemical vapor deposition (CD-CVD) method using hexamethyldisiloxane as amorphous silica source, and the effect of the mesoporous intermediate layer and the CD-CVD process temperature on the hydrothermal stability of the amorphous silica membranes were studied. A mesoporous amorphous silica intermediate layer with a mean pore size of 20 nm was synthesized on a macroporous α-Al_2O_3 support. Under a hydrothermal condition at 500°C by maintaining steam-nitrogen mixed gas, the mesoporous amorphous silica intermediate layer exhibited an excellent stability, while the conventional sol gel-derived mesoporous γ-Al_2O_3 intermediate layer showed considerable degradation. The improvement in the hydrothermal stability at 500°C of the hydrogen-permselective amorphous silica membrane was successfully achieved by high-temperature synthesis at 700°C of the CD-CVD-derived microporous amorphous silica membrane on the porous α-Al_2O_3 support having the hydrothermally stable amorphous silica intermediate layer. Further study on the microstructure observations and evaluation of activation energies for the hydrogen permeation through the amorphous silica membranes were performed, and the results are shown and discussed from a viewpoint to achieve further hydrothermal stability improvement for further applications to hydrogen production processes.

Key-words : Amorphous silica, Microporous membrane, CVD, Hydrogen, Gas separation, Alumina, Ceramic membrane

[Received July 22, 2013; Accepted October 20, 2013]

1. Introduction

Hydrogen is expected as one of the new generation clean energy sources which can solve concerns such as global warming and exhaustion of fossil fuels. Thus hydrogen separation membranes which can be utilized to hydrogen production, recovery and storage systems have paid much attention. Particularly, the application of high-temperature membrane reactors to steam reforming step is considered to be attractive due to their potential to achieve the equivalent conversion efficiencies as those attained in conventional reactors at a significantly lower temperature of about 500°C.[1),2)]

Various materials including metal,[3)] organic,[4)] inorganic and their compounds[5)] have been studied to develop high-performance membranes for hydrogen separation. Especially, amorphous silica membranes exhibit an excellent hydrogen perm-selectivity, which could be achieved by the molecular sieve-like functionality of the in-situ formed microporous amorphous silica network having a suitable mean pore diameter of approximately 0.3 nm.[6)] Therefore membrane forming processes of amorphous silica such as sol–gel,[7),8)] chemical vapor deposition (CVD)[9),10)] and polymer pyrolysis[11)] routes have been studied.

Typical amorphous silica-based membranes studied in the past[9),12)–20)] are listed in **Table 1**, and their multi-layered structure is shown in **Fig. 1**. Generally, the microporous amorphous silica membrane can be fabricated on a macroporous α-Al_2O_3 support, and an important structural feature is an intermediate layer i.e., a mesoporous ($2\,\text{nm} < \varphi < 50\,\text{nm}$) thin layer, which is placed between the layer of a hydrogen perm-selective microporous silica-based membrane on the upper side and the surface of a macroporous α-Al_2O_3 support on the inner side. To synthesize amorphous silica membranes with high hydrogen permselectivity, it is important to form a fine intermediate layer without defects and cracks. Recently, hydrogen permselectivity of amorphous silica membranes were dramatically improved, which could be achieved by progress of the membrane forming processes as well as by the improvement of the intermediate layer forming processes.[21)]

Sol–gel derived γ-Al_2O_3 is often used as the material for the mesoporous intermediate layer, because γ-Al_2O_3 maintains high surface area after the sintering at 600°C, and the pore diameter of the γ-Al_2O_3 can be controlled in the mesopore range.

In the above-mentioned steam reforming process, high operation temperatures are necessary while the reaction atmosphere contains considerable amounts of steam. Thus, the membranes must be sufficiently stable in environments of both increased temperature and containing steam. Recently, Zahir et al. studied hydrothermal stability of the mesoporous γ-Al_2O_3 intermediate layer, and observed the apparent increase in the pore size of the γ-Al_2O_3 by exposure of steam at 500°C, while La_2O_3 doped Ga_2O_3–Al_2O_3 solid solution was found to be significantly stable.[22),23)] Then, CeO_2–ZrO_2–Al_2O_3 nanocomposite[24)] and nickel (Ni)-doped γ-Al_2O_3[25)] were found as potential candidate materials for developing stable mesoporous intermediate thin layer under the hydrothermal condition at 500°C.

In this work, a mesoporous amorphous silica intermediate layer has been synthesized on a macroporous α-Al_2O_3 support using

† Corresponding author: K. Miyajima; E-mail: keita-miyajima@n.noritake.co.jp

DOI http://dx.doi.org/10.2109/jcersj2.121.992

Table 1. Typical amorphous silica-based membranes studied in the past

Macroporous support	Mesoporous intermediate layer	Microporous membrane	Membrane syn. method	Ref.
Porous Vycor glass	—	Amorphous silica	CVD	9)
α-Al_2O_3	γ-alumina	Amorphous silica	Sol–gel	12)
α-Al_2O_3	γ-alumina	Amorphous silica	CVD	13)
α-Al_2O_3	SiO_2–ZrO_2	Ni-doped amorphous silica	Sol–gel	14)
α-Al_2O_3	γ-alumina	Amorphous silica	CVD	15)
α-Al_2O_3	γ-alumina	Amorphous silica	CVD	16)
α-Al_2O_3	γ-alumina	Silica alumina	CVD	17)
α-Al_2O_3	γ-alumina	Silica titania	CVD	18)
α-Al_2O_3	γ-alumina	Silica alumina	CVD	19), 20)

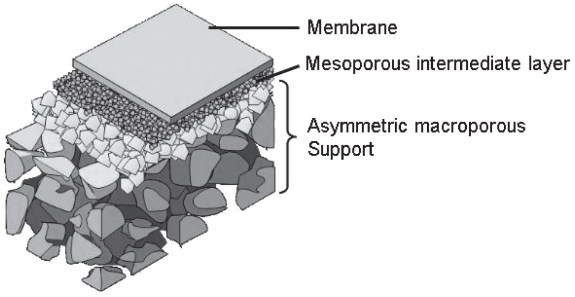

Fig. 1. Typical multi-layered structure of amorphous silica membranes for hydrogen separation.

commercially available nanometer-sized colloidal silica particles. It is expected to be essential that the hydrothermal stability of the microporous amorphous silica membrane be improved by adjusting thermo-mechanical properties such as coefficient of thermal expansion, or harmonizing further densification behavior between the mesoporous intermediate layer and the microporous amorphous silica membrane.

The hydrothermal stability of the mesoporous amorphous silica intermediate layer was studied by comparing the degradation behavior under the hydrothermal condition at 500°C of the conventional mesoporous γ-Al_2O_3 intermediate layer. Then, amorphous silica membrane was formed on a macroporous α-Al_2O_3 support with a mesoporous intermediate layer of γ-Al_2O_3 or amorphous silica by using the counter diffusion CVD (CD-CVD) method.

The hydrothermal stability of amorphous silica membranes was evaluated at 500°C for 200 h by measuring the hydrogen and nitrogen gas permeances under the hydrothermal condition by maintaining steam-nitrogen mixed gas.

2. Experimental procedure

2.1 Synthesis and evaluation of mesoporous intermediate thin layer

The macroporous α-Al_2O_3 tubular support was developed by Noritake Co., Limited.[26),27)] This support was asymmetric and composed of macroporous α-Al_2O_3 (mean pore diameter: 700 nm, porosity: 35–40%) and a fine outer surface thin layer (mean pore diameter: 70 nm, porosity: 35–40%, thickness: approximately 100 μm). The diameter and length of the tubular support was 10 and 100 mm, respectively. Each edge end of the support was coated with dense glass glaze not to make leakage at the connection parts in the subsequent process of amorphous silica membrane formation by the CD-CVD method.

The mesoporous γ-Al_2O_3 intermediate layer was formed on the tubular support according to the published procedures.[26)–28)] 0.05 M of aluminium-tri-sec-butoxide (ASTB, Aldrich USA) was dissolved in isopropyl alcohol dehydrated (Wako chemical, Japan). Then, boehmite (γ-AlOOH) sol was prepared by reacting the 0.1 M alkoxide solution with distilled water at 90°C. The reaction mixture was maintained at 90°C for at least 1 h to remove the isopropyl alcohol and butanol by evaporation. The mixture was cooled down to room temperature and peptized with 1 M HNO_3 at a pH of about 3. During the synthesis, the sol was vigorously stirred. The peptized mixture was refluxed at 90°C for 12 h. Resultant boehmite sol was diluted with 3.5 wt % water solution of polyvinylalcohol (PVA #500, Kanto chemical, Japan), and coated on the tubular support. The concentration of the boehmite sol was 0.025 mol/l. The coated support was calcined at 600°C in air. After the first calcination, 0.005 mol/l boehmite sol, diluted by distilled water, was coated on the support and calcined at 600°C in air.

For the mesoporous amorphous silica intermediate layer synthesis, commercially available silica colloidal sol (PL-1, Fuso chemical, Japan) having average particle diameter of 15 nm was used. The silica sol was diluted with 10 wt % water solution of polyvinylalcohol (PVA #500, Kanto chemical, Japan), and 1wt % silica sol was coated on the macroporous α-Al_2O_3 tubular support, then calcined at 800°C in air. After the first calcination, 0.5 wt % silica sol, diluted by distilled water, was coated on the support and calcined at 800°C in air.

For the pore size distribution measurements, 60°C-dried boehmite sol and silica sol were calcined at 600 and 800°C, respectively. Then, the pore size distribution of the as-calcined samples was measured by the nitrogen adsorption method (BELSORP max, BEL JAPAN Inc.). The mean pore diameters of mesoporous γ-Al_2O_3 and amorphous silica were determined to be 4 and 20 nm, respectively. Hereafter, the macroporous α-Al_2O_3 tubular support with the mesoporous intermediate thin layer of γ-Al_2O_3 and that of amorphous silica were named ALG04 and ALS20, respectively.

Hydrothermal stability tests were performed on the tubular support samples, ALG04 and ALS20. **Figure 2** shows the experimental apparatus used for the hydrothermal stability test and amorphous silica membrane synthesis by the CD-CVD method. The sample was settled in the vessel, and the each end of the sample was sealed by carbon ferrules (GL Science, Japan). Nitrogen gas containing water vapor was supplied to outer side of the tubular sample support using a bubbler. The flow rates at room temperature of nitrogen and water vapor were 200 and 18 ml/min, respectively. Inner side of the tubular sample support, nitrogen was supplied as a sweeping gas with a flow rate of 200 ml/min at room temperature. The tubular sample support was heated by electronic furnace at 500°C. The hydrothermal stability test was performed for 50 h, and the permeances of hydrogen (H_2) and nitrogen (N_2) were measured during the test. Under the same test condition mentioned above, the 600°C-calcined

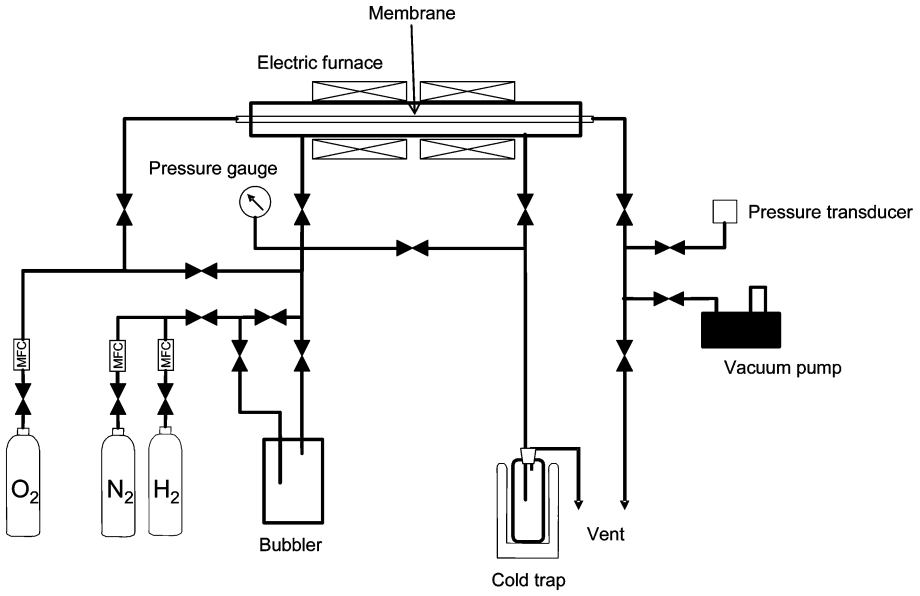

Fig. 2. Experimental apparatus for hydrothermal test and amorphous silica membrane synthesis.

Table 2. Amorphous silica membranes synthesized by the CD-CVD method

Name	CD-CVD condition			Membrane support			
	Formation	Gas flow rate/ml·min^{-1}		Mesoporous intermediate layer		Macroporous support*	
	Temp./°C	N_2	O_2	Name	Material (d_{50}/nm)	Material	Porosity/%
G600	600	200	200	ALG04	γ-Al_2O_3 (4)	α-Al_2O_3	35–40
S600	600	200	40	ALS20	Amorphous silica (20)	α-Al_2O_3	35–40
S700	700	200	40	ALS20	Amorphous silica (20)	α-Al_2O_3	35–40

*Asymmetric tubular support composed of macroporous α-Al_2O_3 (d_{50}: 700 nm, porosity: 35–40%) and a fine outer surface thin layer with a thickness of approximately 100 mm (d_{50}: 70 nm, porosity: 35–40%).

mesoporous γ-Al_2O_3 and 800°C-calcined amorphous silica samples were also exposed to the steam for 50 h, then pore size distributions before and after the steam exposure were compared.

2.2 Synthesis and evaluation of amorphous silica membranes

Hexamethyldisiloxane (HMDS) was used as the silica precursor. The porous support with a mesoporous intermediate thin layer was settled in the vessel shown in Fig. 2, and the each end of the porous support was sealed by carbon ferrules (GL Science, Japan). The saturated vapor of HMDS was introduced to the vessel using N_2 as a carrier gas. The vaporized precursor was supplied to the outer side of the porous support, while oxygen as the reaction gas was supplied to the inner side of the porous support. The pressures of the outer side and the inner side were carefully kept at 150.2 and 150 kPa, respectively.

Table 2 summarized the synthetic conditions of amorphous silica membranes investigated in this study. The flow rate at room temperature of the reactant oxygen (O_2) gas was fixed as 200 ml/min, while that of N_2 gas carrier for HMDS was controlled to be 200 ml/min for ALG04, and 40 ml/min for ALS20. The membrane formation was studied at 600 and 700°C. Totally, three different amorphous silica membranes, G600, S600 and S700 were synthesized; G600 was synthesized at 600°C on the macroporous alumina support having the mesoporous γ-Al_2O_3 intermediate layer, while S600 was synthesized at 600°C on the macroporous alumina support having the mesoporous amorphous silica intermediate layer. S700 was synthesized at 700°C on the same support used for S600.

The single gas permeances of H_2 and N_2 were evaluated for the as-synthesized amorphous silica membranes. Microstructure of the multi-layered membranes was observed by a field emission scanning electron microscope (FE-SEM, Model S-4700, Hitachi, Japan)

The hydrothermal stability tests at 500°C were performed on the amorphous silica membranes under the same condition as described in the section 2.1. During the 200 h test, the H_2 and N_2 permeances through the membrane were measured.

3. Results and discussion

3.1 Hydrothermal stability of mesoporous intermediate thin layer

Figure 3 shows the gas permeance changes during the hydrothermal test of ALG04 and ALS20. The H_2 permeances through as-synthesized ALG04 and ALS20 were the same 10^{-5} mol Pa^{-1} m^{-2} s^{-1} order (1.7×10^{-5} mol Pa^{-1} m^{-2} s^{-1} and 1.1×10^{-5} mol Pa^{-1} m^{-2} s^{-1}, respectively). However, the H_2 and N_2 permeances through ALG04 drastically increased during the initial several hours, then continuously increased with increasing the steam exposure time, while those through ALS20 kept almost the initial values even after 50 h.

Figure 4 shows the change of pore size distribution measured for the mesoporous γ-Al_2O_3 and amorphous silica before and after the hydrothermal treatment under the same condition. The pore size distribution of γ-Al_2O_3 after the hydrothermal treatment shows an apparent sift toward larger size, which is well consistent with the results of our previous study on the hydrothermal stability of γ-Al_2O_3 mesoporous intermediate layer by using a perm

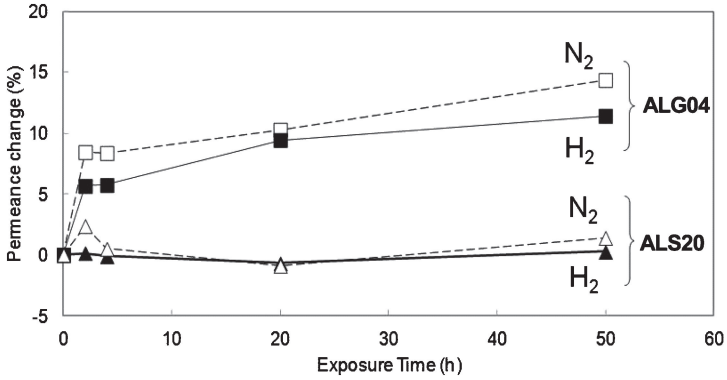

Fig. 3. Gas permeance changes observed for γ-Al_2O_3 tubular porous support sample with a mesoporous intermediate thin layer during the hydrothermal test at 500°C for 50 h.

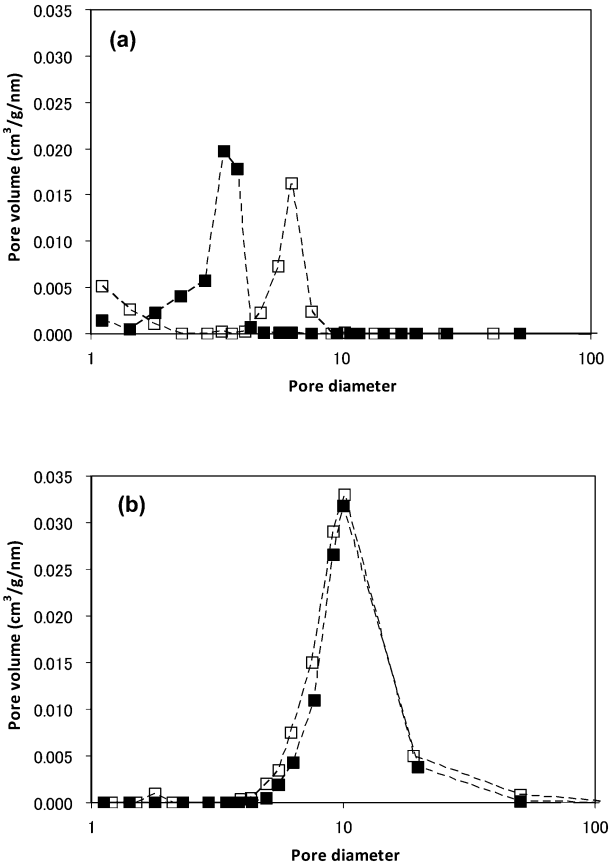

Fig. 4. Pore size distribution of mesoporous (a) γ-Al_2O_3 and (b) amorphous silica. ■: Before and □: After hydrothermal test at 500°C for 50 h.

porometer.[22)–24)] On the other hand, the mesoporous amorphous silica was found to be stable without degradation, and kept the initial pore size distribution under the hydrothermal condition up to 50 h, which could contribute to the stable gas permeation behaviors observed for ALS20 during the 50 h hydrothermal test.

3.2 Microstructure and hydrothermal stability of amorphous silica membranes

Cross sectional FE-SEM images of G600 are shown in **Fig. 5**(a). Defect-free thin layer with a thickness of approximately 2 μm was formed on the outer surface of the macroporous α-Al_2O_3 support, and it is estimated that the amorphous silica membrane was deposited within the mesoporous γ-Al_2O_3 to form a fine composite surface thin layer [Fig. 5(b)].

S600 and S700 also presented the same structural feature, and the surface thin layer of these samples is considered to be composed of mesoporous amorphous silica derived from colloidal silica particles and CVD-derived microporous amorphous silica. As typical observation results, cross-sectional FE-SEM images of S700 are shown in Figs. 5(c) and 5(d).

The gas permeances through the as-synthesized amorphous silica membranes are shown in **Fig. 6**. As-synthesized S600 exhibited a H_2 permeance of 5.60×10^{-7} mol Pa^{-1} m^{-2} s^{-1} with a selectivity [$\alpha(H_2/N_2)$] of 255. The values were comparable with those of as-synthesized G600. When the amorphous silica membrane was formed at higher temperature of 700°C (S700), the H_2 permeance slightly decreased to 3.77×10^{-7} mol Pa^{-1} m^{-2} s^{-1}, while the $\alpha(H_2/N_2)$ drastically increased to 829.

During the hydrothermal stability test, the membrane sample having the mesoporous γ-Al_2O_3 intermediate layer, G600 showed considerable performance degradation associated with an immediate decrease in H_2 permeance within 20 h, and a rapid increase in N_2 permeance within 100 h. Then, both the H_2 and N_2 permeances slightly increased with increasing the steam exposure time. After 200 h, the H_2 permeance and the $\alpha(H_2/N_2)$ were 1.31×10^{-7} mol Pa^{-1} m^{-2} s^{-1} and 5.6, respectively [Fig. 6(a)].

The membrane sample having the mesoporous amorphous silica intermediate layer, S600 [Fig. 6(b)] also showed performance degradation, however the gas permeation behaviors were different from those of G600. Especially, such a large increase in the N_2 permeance was not observed within the 100 h, and the N_2 permeance gradually increased with increasing the steam exposure time, while the H_2 permeance decreased consistently with the time.

Compared with S600, the hydrothermal stability of the 700°C-formed S700 was found to be improved, and the changes in the H_2 and N_2 permeances during the first half of the hydrothermal stability test were much suppressed, then, the permeances were turned to be stable. Finally after 200 h, the H_2 permeance and $\alpha(H_2/N_2)$ were 6.54×10^{-8} mol Pa^{-1} m^{-2} s^{-1} and 28.6, respectively.

The activation energies for the H_2 permeations through S600 and S700 were calculated from the arrhenius plots of H_2 permeances measured at temperatures ranging from 200 to 500°C, and plotted in Fig. 7. The initial activation energies of S600 and S700 were 6.5 and 11.5 kJ/mol, respectively. The value of S600 was compatible with that previously reported for the CVD-derived amorphous silica membrane at H_2 permeation temper-

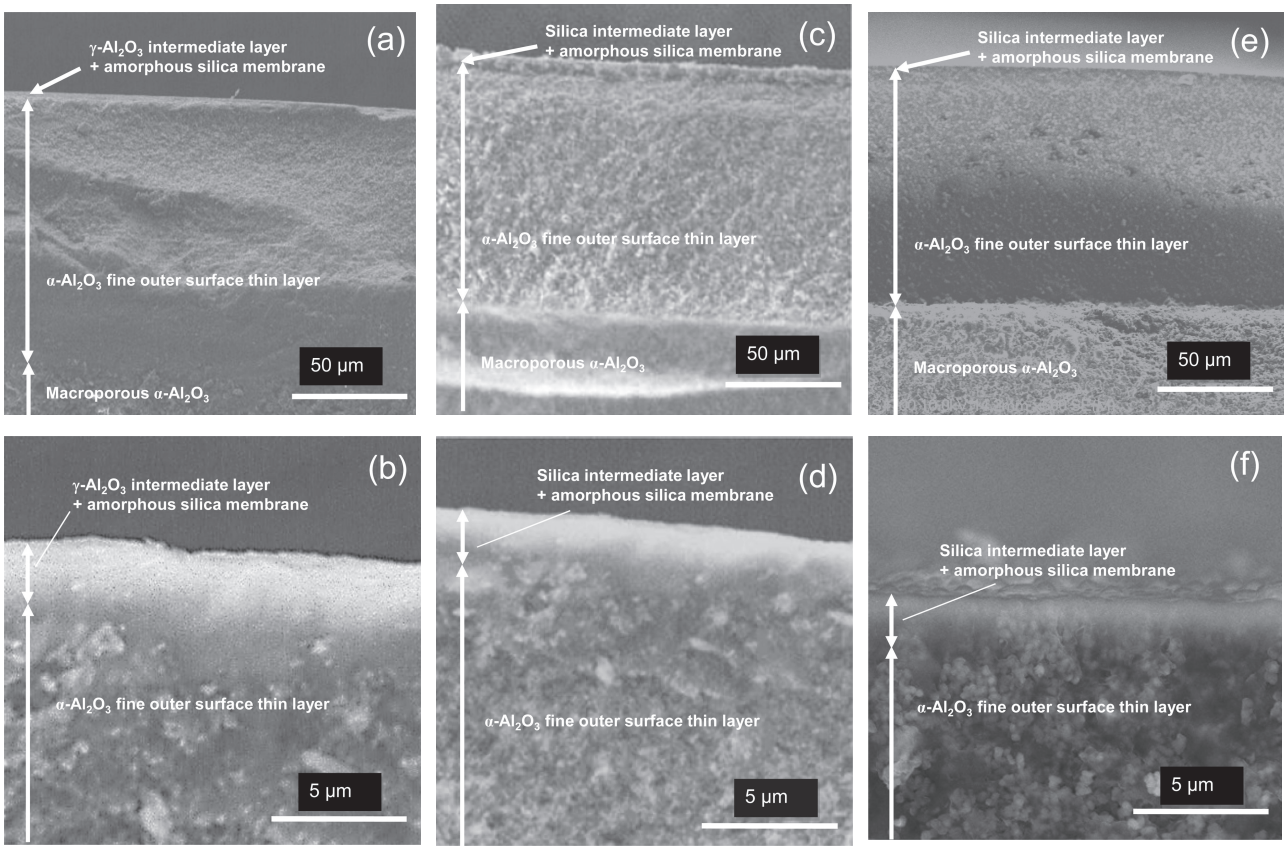

Fig. 5. Cross sectional FE-SEM images of amorphous silica membranes. (a), (b): G600, and (c), (d): S600 and (e), (f): S700.

atures in the range of 300 to 500°C,[27] while that of S700 was similar to those previously reported for the CVD-derived amorphous silica membranes at H_2 permeation temperatures in the range of 100 to 300°C[16] or to 100 to 600°C.[28),29]

As shown in **Fig. 7**, the activation energies for the H_2 permeations through S600 and S700 decreased during the steam exposure time up to 50 h, then, slightly increased to reach 19.8 and 18.0 kJ/mol, respectively. This behavior was well consistent with the decreasing behavior during the hydrothermal stability test of the H_2 permeation through S600 and S700 shown in Fig. 6(b). These results indicate that steam-induced densification of the CD-CVD-derived amorphous silica network occurred during the hydrothermal stability test.

In the case of G600, larger gas molecules like N_2 (0.368 nm) could not permeate ideal microporous amorphous silica, but larger defects of pores within the amorphous silica or those such as cracks and gaps at the hetero interface between the mesopore walls of the sol gel-derived γ-Al_2O_3 and the amorphous silica formed by the CD-CVD. On the other hand, the kinetic diameter of steam molecule (0.265 nm) is smaller than that of H_2 (0.289 nm), and steam could permeate through the microporous amorphous silica to reach the mesoporous intermediate layer. Thus, in addition to the steam-induced densification of the CD-CVD-derived amorphous silica, steam-induced pore growth of the mesoporous γ-Al_2O_3 intermediate layer in G600 could occur as shown in Fig. 4(a). The considerable degradation of G600 is due to the instability under the hydrothermal condition of both the 600°C-formed amorphous silica and sol gel-derived mesoporous γ-Al_2O_3, which leading to the formation of the larger defects, especially at the hetero interface between the γ-Al_2O_3 and microporous amorphous silica. As a result, the N_2 permeance through G600 rapidly increased by the permeation through the defects of gaps after steam exposure for 20 h [shown in Fig. 6(a)].

During the hydrothermal stability test, the steam-induced densification of amorphous silica mesopore wall could be also occurred to some extent, however as shown in Fig. 4(b), little change was observed for the pore size distribution of the mesoporous amorphous silica intermediate layer in S600, and such defect formations suggested for G600 could be suppressed. Thus, the rapid increase in the N_2 permeance was not observed after the 20 h steam exposure.

Compared with as-synthesized S600, as-synthesized S700 showed the lower H_2 permeance with much better H_2 permselectivity, and the higher activation energy for the H_2 permeation. The apparent H_2 permselectivity improvement observed for the S700 could be achieved by suppressing larger defect formations. The activation energy evaluated for the membranes depends on the energy bottleneck of the H_2 diffusion through the amorphous silica network. Generally, denser amorphous silica network exhibits lower H_2 permeance with higher activation energy. Therefore, these results revealed that the amorphous silica formed at higher temperature of 700°C was composed of denser amorphous network with reduced amount of the larger defects. This could suppress the defect formations induced by the rapid densification of the amorphous silica detected within the initial 50 h of the immediate increase in the activation energy for the H_2 permeation through S600. Then, S700 exhibited relatively stable gas permeation properties.

In this study, hydrothermally stable mesoporous amorphous silica intermediate layer was used for evaluating hydrothermal

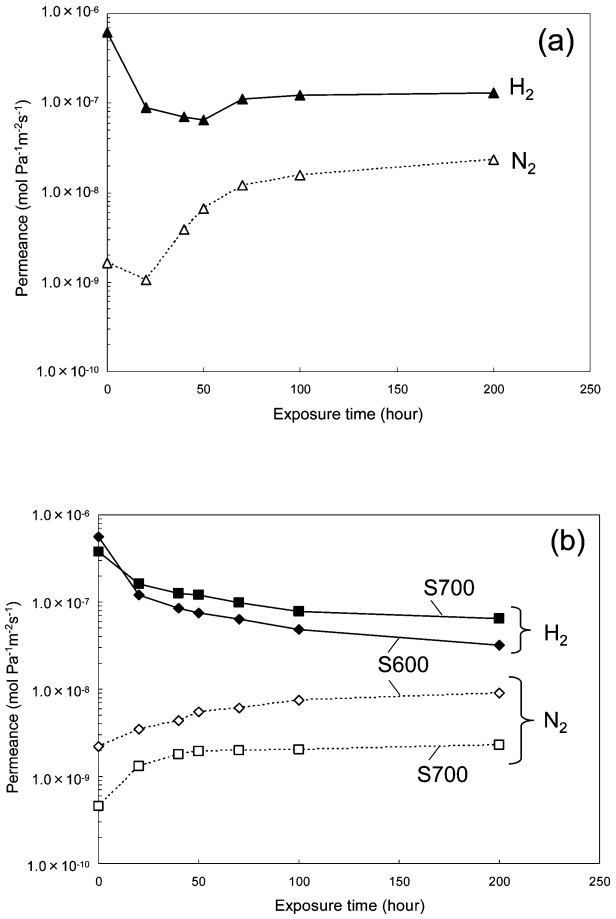

Fig. 6. H_2 and N_2 gas permeation behaviors during the hydrothermal stability test at 500°C. Test sample membranes: (a) G600, and (b) S600 and S700.

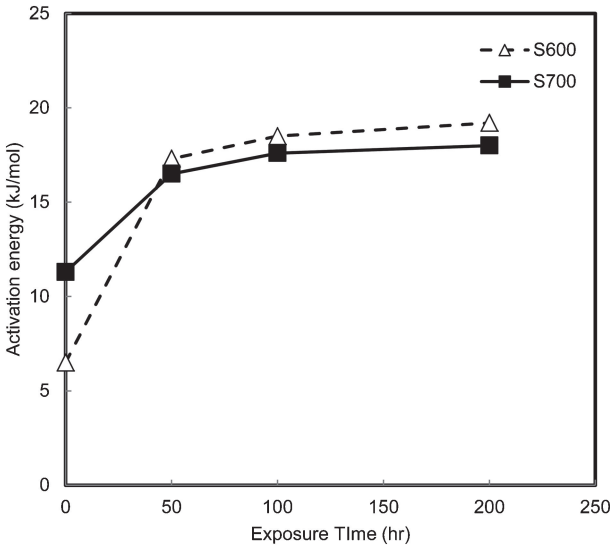

Fig. 7. Activation energy for H_2 permeation through amorphous silica membranes, S600 and S700 as a function of steam exposure time at 500°C.

stability of microporous amorphous silica membranes synthesized by the CD-CVD method. By direct comparison with the membrane having mesoporous γ-Al_2O_3 intermediate layer which was unstable under the hydrothermal condition, the influence of the intrinsic steam-induced densification of the amorphous silica network on the membrane performance degradation under the hydrothermal condition was clearly observed.

4. Summary

In this study, H_2-permselective amorphous silica membranes were synthesized by the CD-CVD method using HMDS as amorphous silica source, and the effect of the mesoporous intermediate layer and the CD-CVD process temperature on the hydrothermal stability of the amorphous silica membranes were studied. The results can be summarized as follows:

(1) A mesoporous amorphous silica intermediate layer with a mean pore size of 20 nm was synthesized on a macroporous α-Al_2O_3 support using commercially available nanometer-sized colloidal silica particles.

(2) The stability test was performed at 500°C for 20 h under the hydrothermal condition by maintaining steam/N_2 mixed gas. The mesoporous amorphous silica intermediate layer exhibited an excellent stability, while the conventional sol gel-derived mesoporous γ-Al_2O_3 intermediate layer showed considerable degradation.

(3) Relatively high-performance was achieved for the 700°C-synthesized membrane on the porous support with the mesoporous amorphous silica intermediate layer, the H_2 permeance and $\alpha(H_2/N_2)$ at 500°C were 3.77×10^{-7} mol Pa^{-1} m^{-2} s^{-1} and 829, respectively.

(4) The hydrothermal stability of the H_2-permselective amorphous silica membranes was evaluated by measuring the H_2 and N_2 gas permeations during the 200 h steam exposure test at 500°C, and the hydrothermal stability of 700°C-synthesized membrane was found to be much higher than those of other 600°C-synthesized membranes.

(5) The membrane formed at higher temperature of 700°C was composed of amorphous silica network with higher density and reduced amount of the larger defects, which could suppress the degradation by steam-induced densification and defect formations under the hydrothermal condition.

References

1) K. Jarosch and H. I. de Lasa, *Chem. Eng. Sci.*, 54, 1455–1460 (1999).
2) E. Kikuchi, *Catal. Today*, 56, 97–101 (2000).
3) E. Kikuchi and S. Uemiya, *Gas separation & Purification*, 5, 261–266 (1991).
4) K. Tanaka, H. Kita, K. Okamoto, A. Nakamura and Y. Kusuki, *J. Membr. Sci.*, 47, 203–215 (1989).
5) M. Kanezashi, K. Yada, T. Yoshioka and T. Tsuru, *J. Membr. Sci.*, 348, 310–318 (2010).
6) W. G. Perkins and D. R. Begeal, *J. Chem. Phys.*, 54, 1683–1694 (1971).
7) R. S. A. de Lange, J. H. A. Hekkink, K. Keizer and A. J. Burggraaf, *J. Membr. Sci.*, 99, 57–75 (1995).
8) K. Kusakabe, S. Sakamoto, T. Saie and S. Morooka, *Sep. Purif. Technol.*, 16, 139–146 (1999).
9) G. R. Gavalas, C. E. Megiris and S. W. Nam, *Chem. Eng. Sci.*, 44, 1829–1835 (1989).
10) A. K. Prabhu and S. T. Oyama, *J. Membr. Sci.*, 176, 233–248 (2000).
11) Y. Iwamoto, K. Sato, T. Kato, T. Inada and Y. Kubo, *J. Eur. Ceram. Soc.*, 25, 257–264 (2005).
12) B.-K. Sea, K. Kusakabe and S. Morooka, *J. Membr. Sci.*, 130, 41–52 (1997).
13) S.-I. Nakao, T. Suzuki, T. Sugawara, T. Tsuru and S. Kimura, *Microporous Mesoporous Mater.*, 37, 145–152 (2000).
14) M. Kanezashi and M. Asaeda, *J. Membr. Sci.*, 271, 86–93

(2006).
15) M. Nomura, T. Nagayo and K. Monma, *J. Chem. Eng. Jpn.*, **40**, 1235–1241 (2007).
16) Y. Ohta, K. Akamatsu, T. Sugawara, A. Nakao, A. Miyoshi and S.-I. Nakao, *J. Membr. Sci.*, **315**, 93–99 (2008).
17) Y. Gu, P. Hacarliouglu and S. T. Oyama, *J. Membr. Sci.*, **310**, 28–37 (2008).
18) Y. Gu and S. T. Oyama, *J. Membr. Sci.*, **345**, 267–275 (2009).
19) M. Amanipour, A. Safekordi, E. G. Babakhani, A. Zamanian and M. Heidari, *J. Membr. Sci.*, **423–424**, 530–535 (2012).
20) M. Amanipour, A. Safekordi, E. G. Babakhani, A. Zamanian and M. Heidari, *Int. J. Hydrogen Energy*, **37**, 15359–15366 (2012).
21) Y. Iwamoto, *J. Ceram. Soc. Japan*, **115**, 947–954 (2007).
22) M. D. H. Zahir, K. Sato and Y. Iwamoto, *J. Membr. Sci.*, **247**, 95–101 (2005).
23) Md. Hasan Zahir, K. Sato, H. Mori, Y. Iwamoto, M. Nomura and S. Nakao, *J. Am. Ceram. Soc.*, **89**, 2874–2880 (2006).
24) Md. H. Zahir, Y. Ikuhara, K. Sato, S. Fujisaki, T. Nagano and Y. Iwamoto, *J. Mater. Res.*, **22**, 3201–3209 (2007).
25) T. Nagano, K. Sato, T. Saitoh and S. Takahashi, *J. Ceram. Soc. Japan*, **117**, 832–835 (2009).
26) Y. Yoshino, T. Suzuki, B. N. Nair, H. Taguchi and N. Ito, *J. Membr. Sci.*, **267**, 8–17 (2005).
27) Y. Yoshino, Y. Ando, H. Taguchi and N. Ito, *Kagaku Kogaku Ronbunshu*, **34**, 242–248 (2008).
28) B. N. Nair, K. Keizer, T. Ohkubo and S.-I. Nakao, *Adv. Mater.*, **10**, 249–252 (1998).
29) D. Lee, L. Zhang, S. T. Oyama, S. Niu and R. F. Saraf, *J. Membr. Sci.*, **231**, 117–126 (2004).